JOURNAL OF MATERIALS SCIENCE 30 (1995) 4684–4691

Oxidation and corrosion behaviour of mild steel laser alloyed with nickel and chromium

A. S. KHANNA
Corrosion Science and Engineering, Indian Institute of Technology, Bombay 400076, India
A. GASSER, and K. WISSENBACH
Fraunhofer Institute for Laser Technique, Aachen D-52074, Germany
MING LI and V. H. DESAI
Material Science Programme, University of Central Florida 32816–0993, USA
W. J. QUADAKKERS
IRW, Research Centre Juelich, D-52425, Juelich, Germany

Surface alloys were made on mild steel, coated with nickel and chromium using laser surface alloying. Mild steel was coated with a composite layer of nickel and chromium using the plasma technique. This was followed by laser irradiation using a continuous carbon dioxide laser. Oxidation and corrosion behaviour of these alloys was then determined by carrying out oxidation in air at 800 °C and corrosion tests at room temperatures in 1 N H_2SO_4. With a 75 μm layer of nickel and chromium each, it was possible to make surface alloys on mild steel, which had a chromium concentration of 6–7 wt%, but the nickel concentration varied from 10–20 wt%. Oxidation behaviour improved significantly over the as-coated specimen and aqueous corrosion improved considerably.

1. Introduction

Laser surface treatment is currently being considered for variety of applications relating to surface properties modification. Treatment may involve surface melting, such as laser surface alloying, laser glazing or surface hardening, which involves no melting. To date, several studies have illustrated these applications [1–5]. Laser surface alloying is a versatile technique to form surface alloys with different metals, by melting a small portion of the substrate metal and the metal which is needed to be alloyed, either by continuously feeding it to the surface or by being pre-deposited on the surface. It has several advantages: it helps in limiting sometimes a costly and strategic material only to the surface and thus saving huge wastage. Secondly, by limiting the element to the surface, its effective use can be made in improving the surface properties, rather than bulk alloying, where either it is not needed or, if present, interacts with the bulk properties of the material.

Mild steel is used in several day-to-day applications, mainly at ambient temperatures. Its corrosion resistance is very poor. In a moist atmosphere, it can form rust and the reaction continues. Although, mild steel can be used for several applications up to 250–300 °C, poor oxidation resistance restricts its use. If, by some means, the surface composition is altered, favouring the formation of a passive film at ambient temperatures or a protective layer at higher temperatures, its use can be extended to a wide number of applications.

In an earlier work, one of the authors [6] has shown how stainless steel coating on mild steel improves its oxidation resistance. It was shown that by choosing proper laser parameters, it is possible to concentrate the useful alloying elements in the surface layer to improve the corrosion and oxidation resistance. In another work, it was shown that by increasing the surface concentration of chromium in 9Cr–1Mo steel by laser surface alloying, the passivity of the surface was increased [7]. In the present work, it was planned to enrich the surface of mild steel with chromium and nickel by laser surface alloying to improve its corrosion and oxidation resistance.

2. Experimental procedure

Mild steel sheet (50 mm × 50 mm × 2 mm), cleaned using sand blasting, was coated first with 50 μm nickel followed by further 50 μm chromium coating. Pure nickel and chromium powders were used for plasma coatings. The plasma coating parameters were as follows: plasma torch power 20 kW, plasma gas 20 l min^{-1} argon, current 350 A, voltage 25 V, powder feed rate 15 g min^{-1}, powder carrier gas 8 l min^{-1} argon, specimen to torch distance 10 mm.

After plasma coating, the surface appeared very rough, as shown in scanning electron micrographs (Fig. 1a and b). Large pores and an uneven surface are evident from these micrographs. The exact scale thickness after plasma coating, and the microstructure of the substrate, are shown in Fig. 2. The inner nickel coating appears slightly darker than the outer

0022–2461

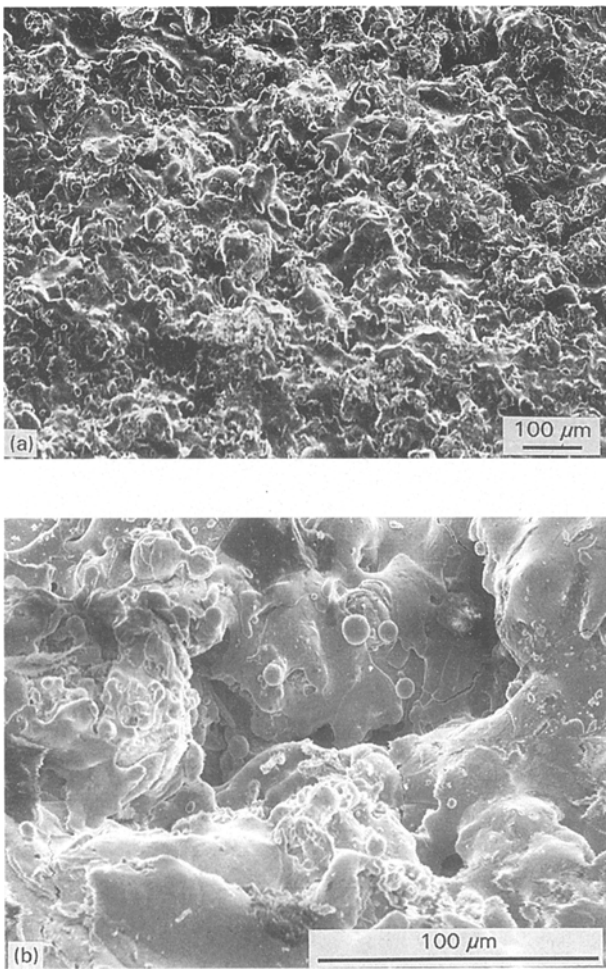

Figure 1 Scanning electron micrographs, showing surface morphology of a plasma-coated sample with nickel and chromium: (a) overall morphology of the coating, (b) pores.

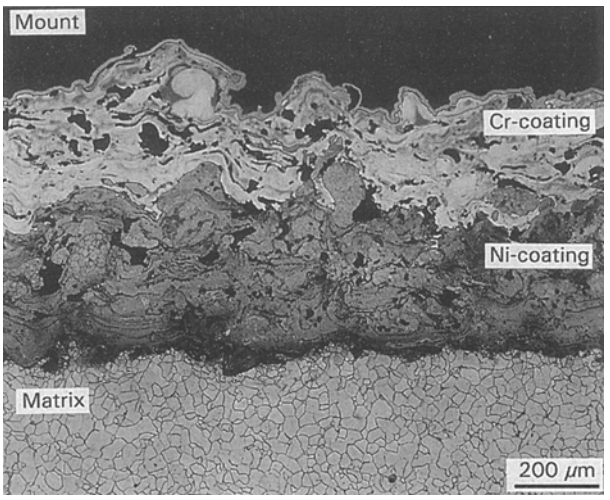

Figure 2 Optical micrograph showing a cross-section of the plasma-coated sample.

chromium coating. The total thickness of the composite layer is about 150 μm and the exact thickness of each layer is about 75 μm each, instead of the planned 50 μm.

Laser treatment was carried out using a 5kW carbon dioxide continuous laser at the Fraunhofer Institute for Laser Technique, Aachen, Germany. A 3 kW laser beam, in line-focus mode (spot size 0.5 mm × 6 mm) was used for irradiation. This gave an energy density of 105 $W cm^{-2}$. The specimens were irradiated under a continuous flowing argon gas stream (flow rate 20 l min^{-1}). The only parameter which was varied during laser irradiation was the sweep speed, from 750–500 mm min^{-1}. This gave an interaction time of 40–60 ms. The designation of the various laser-treated samples, their sweep speed, interaction time and thickness of melt zone achieved, are given in Table I.

Optical micrographs of the cross-section, showing the laser-melted zone and the microstructure of the substrate, are given in Fig. 3. It can be seen that there is a little, but significant, change in the microstructure of the substrate after laser treatment. At higher sweep speed/low interaction time, the heat transferred to the substrate is for short duration. This gives a substrate microstructure which is fine next to the melt zone, followed by higher grain size (Fig. 3a). The formation of carbides at grain boundaries is also evident in the heat-affected zone, in this sample. At the lowest scan speed (higher interaction time), the grain size is refined throughout the substrate matrix, indicating the transfer of heat to the whole cross-section of the specimen (Fig. 3d). At intermediate speeds, the effect is comparatively small.

Oxidation tests were carried out at 800 °C, by exposing the as-coated and laser-treated samples to air in a muffle furnace. Weight gains were measured after a definite interval of time by interrupting the experiment.

Corrosion tests were carried out in 1N H_2SO_4 solution using a potentiodynamic polarization technique. The critical current density, passive current and passive potential range were measured as a function of depth by grinding the samples after each polarization test. The test was carried out by mounting the laser-treated specimen in an epoxy resin making an electric contact on the reverse side of the sample using a copper wire. The anodic polarization test was carried out in 1N H_2SO_4 solution. All the electrode potential measurements were carried out with respect to a saturated calomel electrode (SCE) and the potential scan rate was maintained at 10 mV min^{-1}. The polarization experiments were started from a cathodic potential of -500 mV (SCE) and were continued until transpassivity was attained. Tests were carried out first on the as-treated specimen, without polishing, and were repeated by polishing the surface after each test. Correpsonding levels of chromium and nickel, remaining on the surface, were measured using energy dispersive analysis of X-rays (EDAX). The thickness of the layer removed after each polishing was about 25 μm.

3. Results

3.1. Characterization of laser-treated samples

Surface morphology of the laser-treated specimen (LT1) is given in Fig. 4a and b. A relatively more uniform and dense surface compared to that of the

TABLE I

Sample designation	Sweep speed (mm min^{-1})	Interaction time (ms)	Thickness of laser-melted zone (μm)
LT1	750	40	330
LT2	625	48	400
LT3	575	52	500
LT4	500	60	575

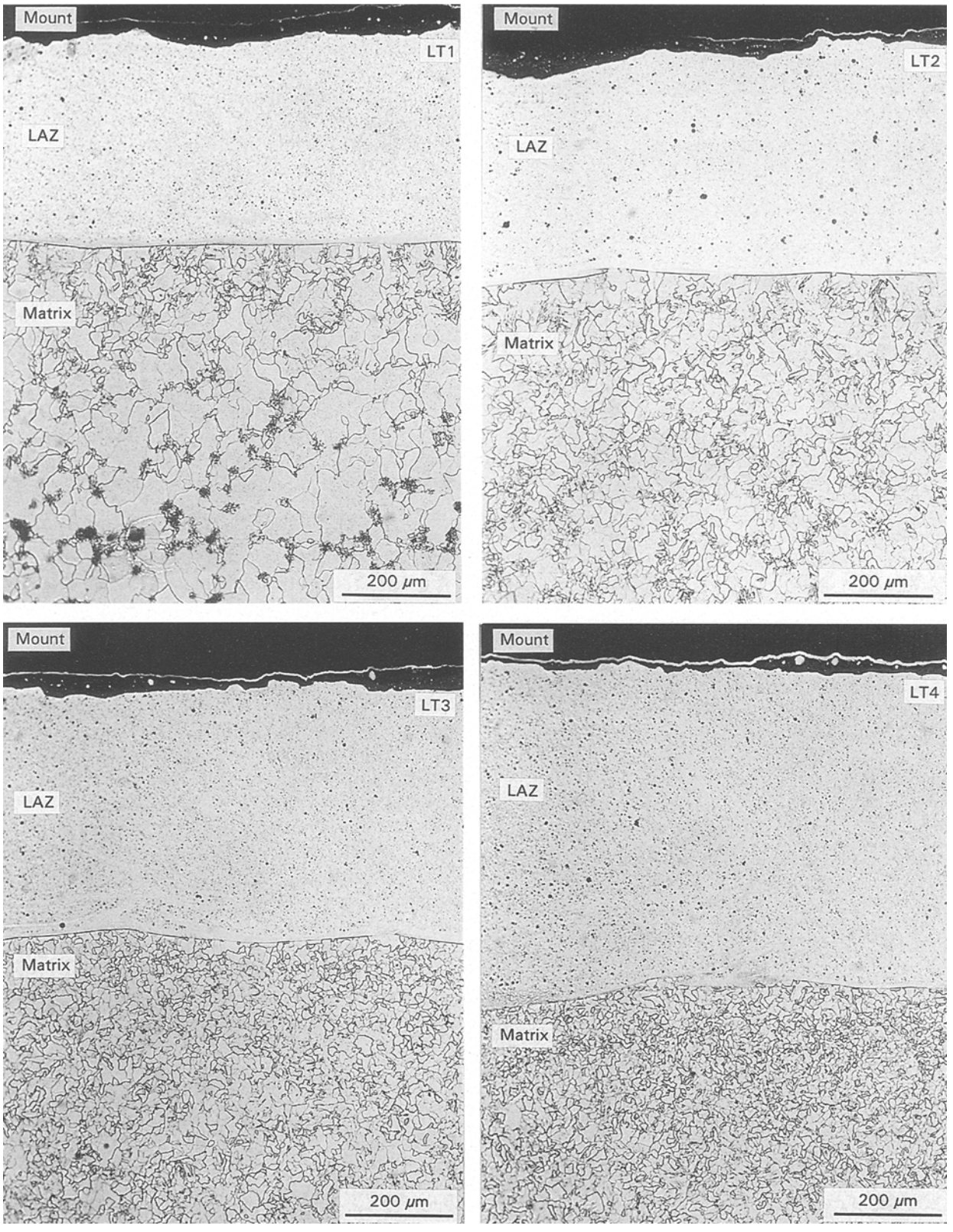

Figure 3 Optical micrographs showing cross-sections of the laser-treated samples; LAZ, laser alloying zone.

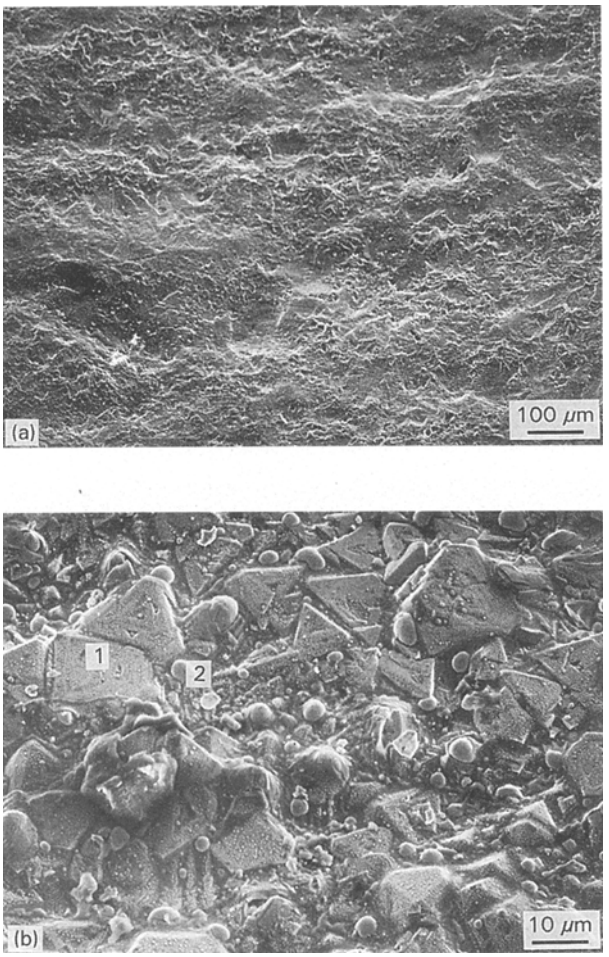

Figure 4 Scanning electron micrograph showing the surface morphology of laser-treated sample LT1: (a) overall morphology, (b) fine structure.

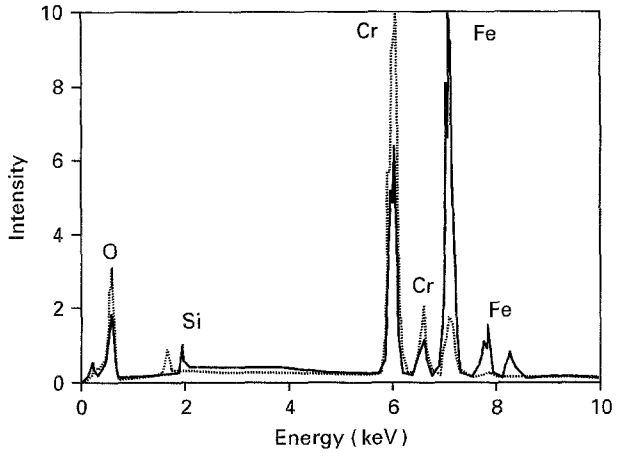

Figure 5 Composition of phases (···) 1 and (—) 2 in Fig. 4b.

as-coated specimen is evident from Fig. 4a. At higher magnification (Fig. 4b), one can see detailed microstructure. The large triangular-shaped particles are chromium rich and are probably chromium oxide formed during laser processing. The small round shaped particles are iron rich with a considerable amount of chromium also. The exact compositions of these two phases are shown in Fig. 5. The overall composition of the laser-treated specimen is chromium rich and has a certain amount of silicon, diffused out from the mild steel matrix along with the iron (Fig. 6). This differs from the as-coated specimen, which has only chromium on the surface.

The surface morphologies of other laser-treated specimens do not differ significantly from LT1. As shown in Fig. 7, the morphology is very similar, except that due to the longer interaction time, the chromia-rich and iron-rich oxides have grown more.

Fig. 8 shows scanning electron micrographs of the cross-section of various laser-treated specimens.

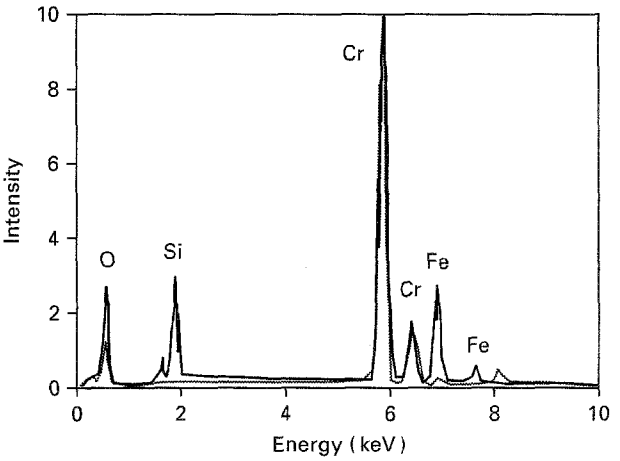

Figure 6 Surface composition of (···) plasma-coated and (—) laser-treated specimen LT1.

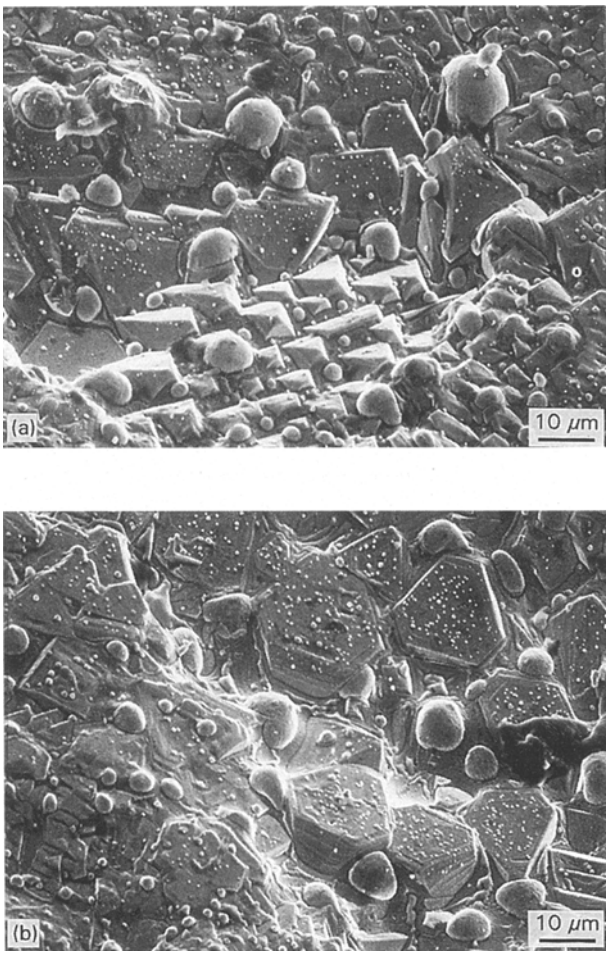

Figure 7 Scanning electron micrographs showing the surface morphologies of laser-treated specimens (a) LT2 and (b) LT4.

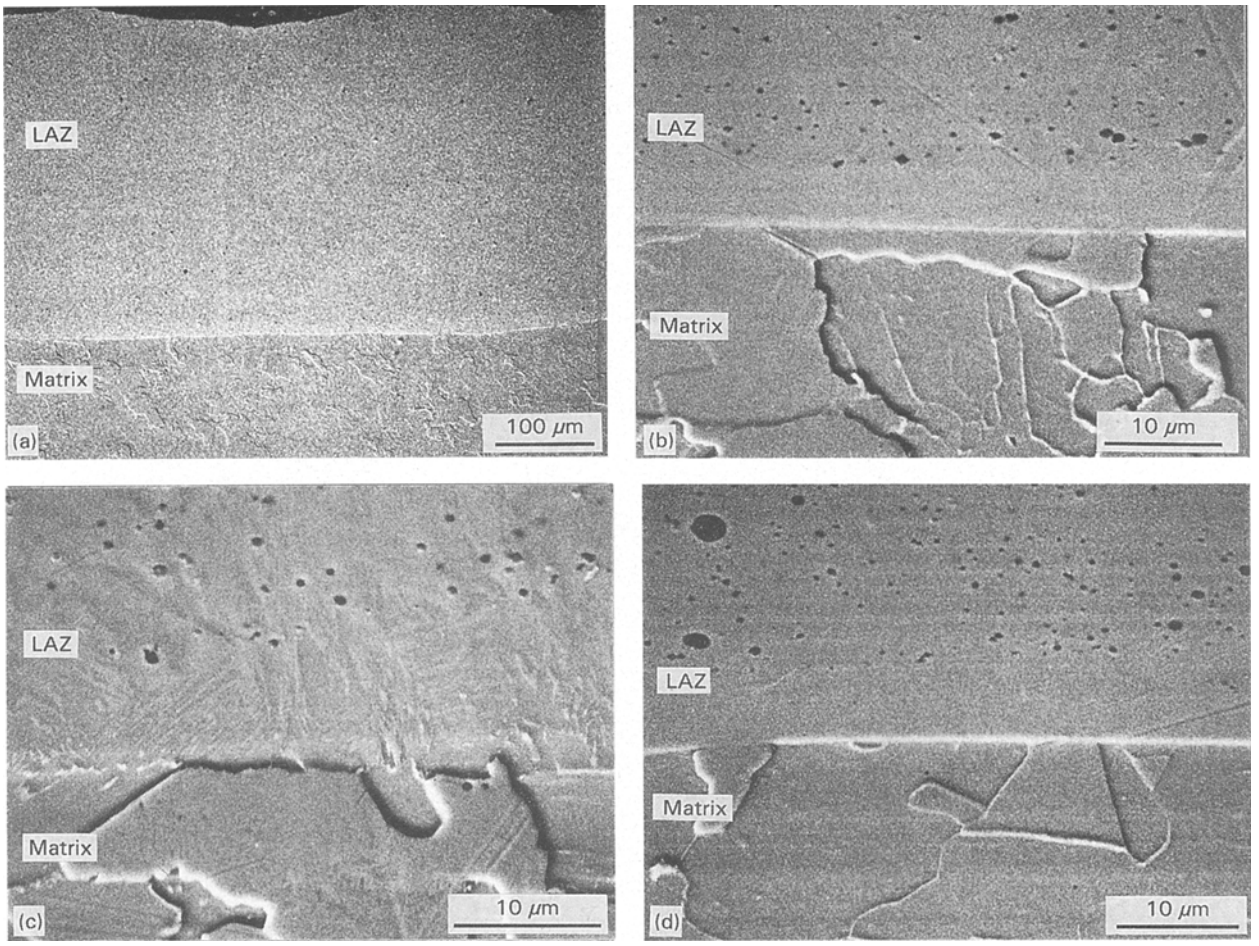

Figure 8 Scanning electron micrographs, showing the cross-section of laser-treated specimens, (a, b) LT1, (c) LT2 and (d) LT4.

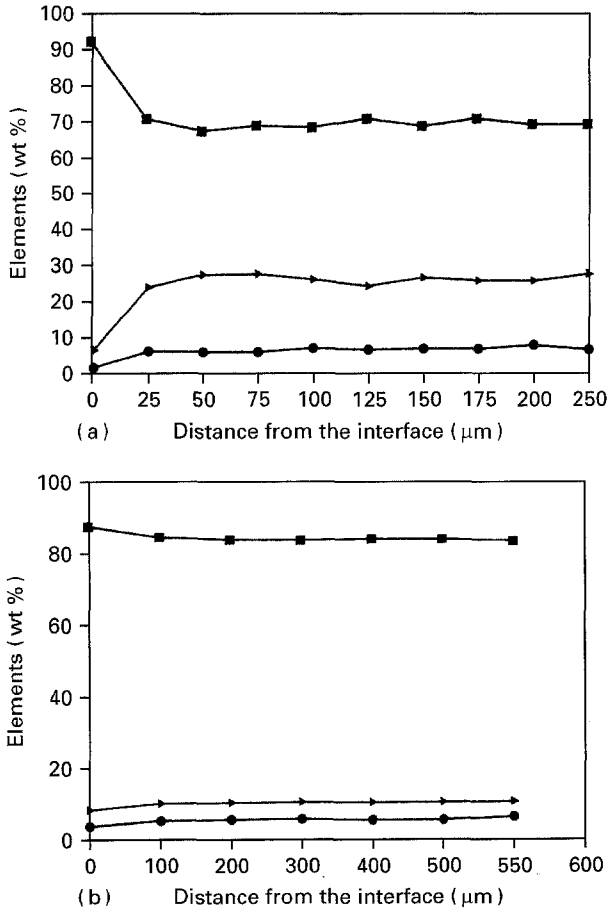

Figure 9 Concentration profiles of (■) iron, (●) chromium and (▶) nickel through the laser melt zone, using quantitative EDX analysis.

A very strong bonding between the substrate and the laser-melted zone with no cracks is evident from these micrographs. The number of pores and perhaps their size is increasing with increase in interaction time.

The distribution of the alloying elements in the laser-melted zone depends very much on the laser parameters. At longer interaction times, more dilution is expected from the coated layer as there is more time available for diffusion to take place. This is evident from the depth-profile results, obtained using quantitative EDAX, shown in Fig. 9 for specimens LT1 and LT4 which differ significantly in their interaction times. The variation in chromium is not very different in the two cases, while there is significant change in the inward diffusion of nickel and outward diffusion of iron. The nickel concentration changes from about 10 wt % in LT1 to about 22 wt % in LT4. Similarly, the iron concentration drops only to 80 wt % for LT1 while the drop is below 70 wt % for LT4.

3.2. Oxidation tests

Oxidation tests, carried out on as-coated and LT1 and LT4 specimens are shown in Fig. 10. It is quite clear from the figure that there is a considerable drop in the oxidation rate when the as-coated specimens are oxidized after laser treatment. However, there is a little change in the oxidation behaviour of the two laser-treated specimens. This is not unexpected. It is well known that nickel does not play a very significant role in the oxidation behaviour, while the chromium level

in the alloy decides its resistance to oxidation. Because there is a small change in the concentration of chromium in the surface layer, no great difference in the oxidation behaviour is expected for the two laser-treated specimens.

3.3 Corrosion tests

Fig. 11 shows the results of polarization test of specimen LT1 in 1N H_2SO_4 solution. The results for the specimens LT1 are given in Fig. 11. Fig. 12 gives the

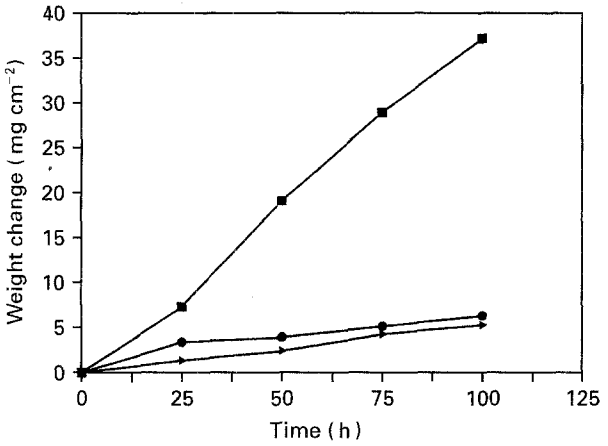

Figure 10 Linear plots of weight gain versus time for the oxidation of (■) as-coated and laser-treated specimens (▶) LT4, and (●) LT2.

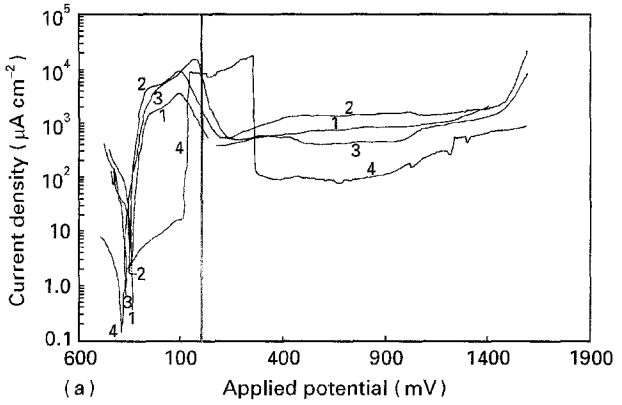

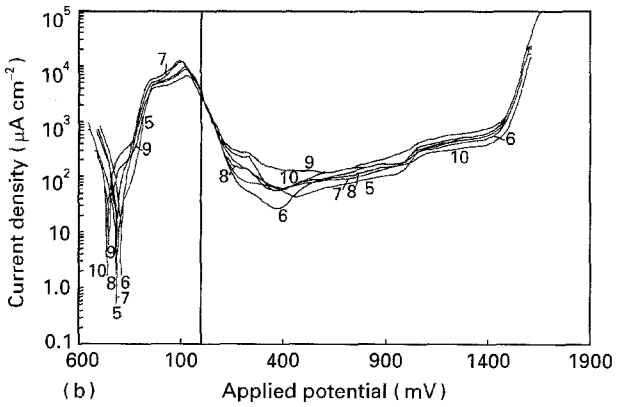

Figure 11 (a, b) Potentiodynamic polarization curves for the sample LT1, treated in 1N H_2SO_4 solution. (1) 25 μm, (2) 50 μm, (3) 100 μm, (4) 125 μm, (5) 150 μm, (6) 175 μm, (7) 200 μm, (8) 225 μm, (9) 250 μm, (10) 275 μm.

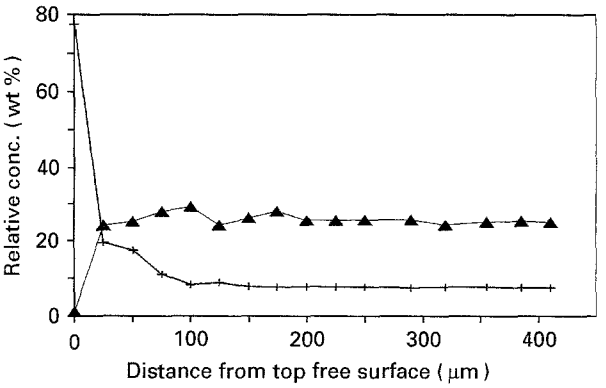

Figure 12 (+) chromium and (▲) nickel profiles on sample LT1, measured using EDAX at various stages during polishing before carrying out the polarization run.

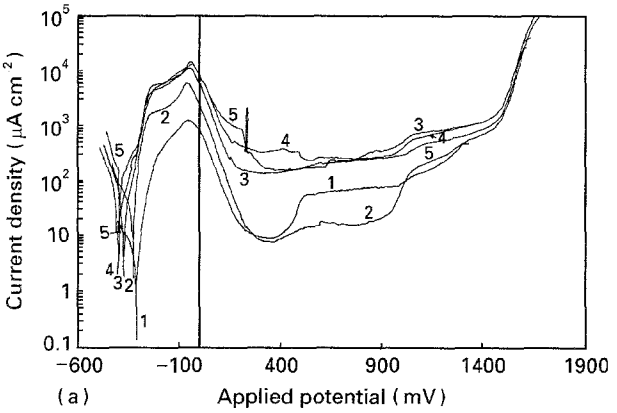

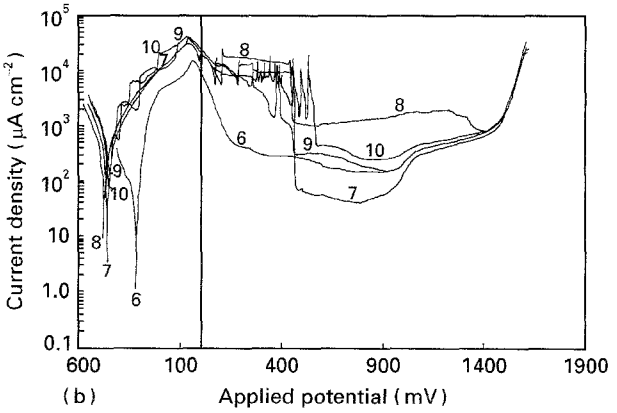

Figure 13 (a, b) Potentiodynamic polarization curves for sample LT4 in 1N H_2SO_4 solution. (1) surface, (2) 25 μm, (3) 50 μm, (4) 75 μm, (5) 100 μm, (6) 125 μm, (7) 175 μm, (8) 200 μm, (9) 225 μm, (10) 250 μm.

corresponding surface chromium and nickel contents at various stages of polishing. A significant change in the polarization plots at various thicknesses in the laser alloy zone indicates change in the corrosion behaviour. The plots 1–4 in Fig. 11, show wide fluctuations, while the plots from 5 onwards are relatively smooth. This could be, perhaps, due to compositional heterogeneity of the laser-alloyed sample, as is obvious from Figs 4 and 7.

Similar results on sample LT4 with corresponding chromium and nickel contents are shown in Figs 13 and 14, respectively. It is evident from the figures that

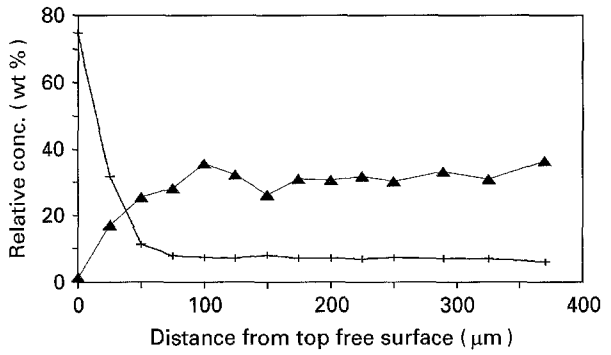

Figure 14 (+) Chromiun and (▲) nickel profiles on sample LT4, measured using EDAX various stages during polishing before carrying out the polarization run.

two important parameters, namely, critical current density (a measure of the corrosion activity, once the passive film is broken) and the passive current density (a measure of the stability of the passive layer) on the surface varies significantly with the corresponding chromium level present at various points in the laser-melted zone. Table II lists these parameters which changed during the polarization test.

4. Discussion

Laser surface alloying of chromium and nickel has improved the oxidation and corrosion behaviour of the mild steel. Although the oxidation behaviour of a plasma-coated specimen shows considerable improvement over that of mild steel, a significant improvement as a result of laser treatment, could be due to much lower porosity, as is evident from Figs 1 and 2 of a plasma-coated layer with the corresponding surface morphology and cross-section after laser treatment (Figs 3 and 4).

Diffusion of chromium and nickel from the coating to the laser-melted zone, and that of iron from the substrate, results in an alloy with reasonably uniform composition on the surface. As is evident from Fig. 9, which shows the depth profiles of the three elements in the matrix, a larger interaction time (lower sweep speed), as in the case of specimen LT4, has diluted more nickel from the laser-melted zone (LMZ) than for the specimen LT1, which has a relatively lower interaction time (higher sweep speed). It is surprising to note that this does not affect the chromium diffusion significantly, whose concentration remains about 6 wt % in both cases, while there is considerable drop in the concentration of nickel in the melt with increase in the interaction time. Perhaps it might be due to the lower melting temperature of nickel compared to that of chromium. Because there is little change in the surface concentration of chromium for the two samples, their oxidation behaviour does not differ considerably, as shown in Fig. 10. Here it can be mentioned that in spite of the fact that the thickness of the plasma-coated chromium is the same as that of nickel, the chromium content of the laser-treated layer is significantly lower than the nickel content. This is due mostly to evaporation of chromium during laser melting, as reported earlier [4].

Corrosion behaviour is usually described by three important parameters; the critical current density, which is the maximum current which is achieved once a passive layer is broken (the lower this value, the more resistant is the material); the passive current density (again lower passive current density leads to better passivation); and similarly, a larger passive range signifies a more stable passive layer under large potential variation. As listed in Table II, both LT1 and LT4 show a critical density on the surface which is lower than that of pure chromium or 9Cr–1Mo steel (reported elsewhere [7]) and it increases as the surface is polished after subsequent runs. A relatively lower critical current density at the as-treated (unpolished) surface might be due to the presence of an atmospheric oxidized layer or due to the high chromium concentration at the surface (Figs 12 and 14). Similarly, the passive current density is also quite low on the surface and is comparable to pure chromium or 9Cr–1Mo steel (10 $\mu A\ cm^{-2}$ for pure chromium and 80 $\mu A\ cm^{-2}$ for 9Cr–1Mo) and this increases with subsequent polishing of the surface for LT4, which can be attributed to the lower chromium at the exposed layer after polishing. For the sample LT1, the slightly lower passive current density, with subsequent tests after each polishing, could not be accounted for from the present results. Passive potential range, however, remains nearly the same during various polishing stages. It is, therefore, possible to achieve a surface which is as

TABLE II Polarization test results

Distance	E_{corr} (mV)		I_{crit} ($\mu A\ cm^{-2}$)		I_{pass} ($\mu A\ cm^{-2}$)		Passive range (mV)	
(μm)	LT1	LT4	LT1	LT4	LT1	LT4	LT1	LT4
0	–	– 315	–	9×10^2	–	8	–	300–1400
25	– 337	– 337	2×10^3	4×10^3	3×10^2	7	100–1200	300–1400
50	– 343	– 376	7×10^3	9×10^3	4×10^2	90	150–1300	200–1400
75	–	– 403	–	9×10^3	–	3×10^2	–	300–1400
100	– 380	– 367	9×10^3	9×10^3	4×10^2	100	150–1400	300–1400
125	– 390	– 317	9×10^3	9×10^3	90	2×10^2	300–1200	200–1400
150	– 408	– 458	5×10^3	–	50	–	400–1400	–
175	– 400	– 482	7×10^3	2×10^4	20	90	400–1400	450–1400
200	– 408	– 433	9×10^3	3×10^4	50	9×10^2	400–1400	400–1400
225	– 400	– 463	9×10^3	3×10^4	50	3×10^2	400–1400	400–1400
250	– 440	– 480	5×10^3	3×10^4	90	5×10^2	400–1400	600–1400

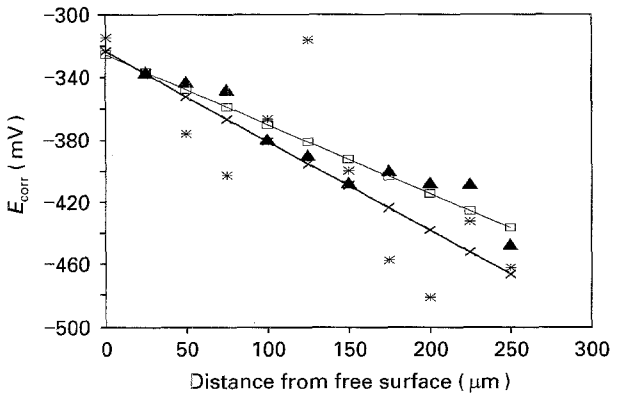

Figure 15 E_{oorr} at various stages during polishing of the laser-treated specimens (▲, □) LT1 and (*, ×) LT4; (□, ×) linear curve fitting.

good as 9Cr–1Mo steel. With successive polishing, the stability of the passive region continues to decrease as shown in Fig. 13, especially for the plots 8 onwards for sample LT4.

One of the important parameters to measure the tendency for corrosion is its equilibrium potential. The more negative is its value, the greater is its tendency to become active. Fig. 15 shows a plot of E_{corr} versus the depth at which the potential was measured after polishing. With subsequent polishing of the surface, its resistance towards corrosion is decreased, in accordance with the observations about the critical current density values, discussed above.

On comparing the results with stainless steels, it can be seen that the behaviour of laser-treated specimens is better than the ferritic stainless steels (18Cr), which require about 10 000 μA cm^{-2} current density to become passivated in comparison to austenitic 18Cr–8Ni stainless steels, requiring a maximum of 100 μA cm^{-2} to acquire passivity, in an oxygenated and non-agitated 1N H_2SO_4 solution [8]. The presence of nickel, therefore, helps in achieving better passivity. The value of I_{crit} achieved in both the samples is below 100 μA cm^{-2}, confirming the usefulness of laser alloying with chromium and nickel. The value on the surface is less than 10 μA cm^{-2}, which increases as the polarization is carried out with subsequent polishing. The results are also comparable to that reported by Chiba *et al.* [4], who carried out similar studies by coating nickel and chromium using electroplating rather than plasma coating as in the present case.

5. Conclusions

Laser surface alloying of chromium and nickel on mild steel has shown significant improvement in the oxidation and corrosion behaviour of the mild steel. A 150 μm thick composite layer of chromium and nickel resulted in a surface composition rich in chromium and nickel, whose corrosion behaviour was better than that of 9Cr-1Mo steel, ferritic stainless steel and was comparable to that of 18Cr–8Ni stainless steel in 1N H_2SO_4 solution. Still better results can be achieved by increasing the chromium concentration in the coating or choosing low-chromium steel as the substrate.

Acknowledgements

The authors thank Mr. F. Ells for helping in carrying out SEM/EDAX analysis, and Mr. Gutzeit for preparing optical micrographs. One of the authors (A.S.K.) acknowledges the International Office for Indo-German bilateral programmes, Research Centre Juelich, for financial support for his stay in Germany whilst carrying out part of this work. The work is a part of a sponsored project from the Department of Science and Technology, India.

References

1. A. GALERIE, M. CAILLET and M. PONS, in "Proceedings of the 10th International Congress on Metallic Corrosion," CECRI, Karai Kudi, India, Vol. IV (Oxford & IBM Pub, ND, 1987) p. 3671.
2. A. S. KHANNA, W. J. QUADAKKERS, H. SCHUSTER, A. GASSER, K. WISSENBACH and E. W. KREUTZ, in "Structure and Reactivity of Surfaces", edited by C. Morterra, A. Zecchena and G. Costa (Elsevier, Amsterdam, 1989) p. 535.
3. J. G. SMEGGIL, A. W. FUNKENBUSCH and N. S. BORNSTEIN, *Thin Solid Films* **119** (1984) 327.
4. A. CHIBA, T. SATO, A. KAWASHIMA, K. ASAMAI and K. HASHIMOTO, *Corros. Sci.* **26** (1986) 311.
5. F. H. STOTT, P. K. N. BARTLETT and G. C. WOOD, *Mater. Sci. Eng.* **88** (1987) 163.
6. A. S.KHANNA, R. K. SINGH RAMAN, E. W. KREUTZ and A. L. E. TERRANCE, *Corros. Sci.* **33** (1992) 949.
7. M. G. PUJAR, R. K. DAYAL, A. S. KHANNA and E. W. KREUTZ, *J. Mater. Sci.* **28** (1993) 3089.
8. M. G. FONTANA, "Corrosion Engineering" 3rd Edn. Materials Science and Engineering Series (McGraw-Hill, USA, 1987) pp. 493–4.

Received 10 March 1994
and accepted 21 Feburary 1995